

FRAGMENTATION IN COULOMB EXPLOSION OF HYDROCARBONS

By

Samuel S. Taylor

Honors Thesis

Submitted to the Faculty of the

Vanderbilt University Department of Physics and Astronomy

in partial fulfillment of the requirements

for

DEPARTMENTAL HONORS

in

PHYSICS

Nashville, Tennessee

Thesis Committee:

Professor Jean-François Paquet , Ph.D.

Professor Raghav Kunnawalkam Elayavalli, Ph.D.

Professor Julia Velkovska, Ph.D.

Copyright © 2024 Samuel S. Taylor
All Rights Reserved

To my brother, John.

ACKNOWLEDGMENTS

I am deeply grateful to everyone who has supported, guided, and encouraged me throughout the past four years. I owe special thanks to Dr. Kálmán Varga for his unwavering support, mentorship, and invaluable guidance during my undergraduate education. His wisdom and encouragement have been instrumental in enabling me to explore and contribute to these research topics.

I would also like to thank all of my professors at Vanderbilt University, particularly those in the Departments of Physics and Astronomy, Computer Science, and Mathematics, for equipping me with the knowledge and skills necessary to engage meaningfully in research. Their dedication and passion have inspired me to continually challenge myself and strive for growth.

A special thanks to Professor Paquet, Professor Raghav, and Professor Velkovska for serving as members of my honors examination committee and to Professor Johns for coordinating the examination.

Lastly, I extend my heartfelt gratitude to my friends and loved ones for their immense support and encouragement every step of the way.

ABSTRACT

Fragmentation dynamics in the Coulomb explosion of hydrocarbons, specifically methane, ethane, propane, and butane, are investigated using time dependent density functional theory (TDDFT) simulations. The goal of this work is to elucidate the distribution of fragments generated under laser-driven Coulomb explosion conditions. Detailed analysis reveals the types of fragments formed, their respective charge states, and the optimal laser intensities required for achieving various fragmentations. The results indicate distinct fragmentation patterns for each hydrocarbon, correlating with the molecular structure and ionization potential. Additionally, the laser parameters that maximize fragmentation efficiency are identified, providing valuable insights for experimental setups. This research advances our understanding of Coulomb explosion mechanisms and offers a foundation for further studies in controlled molecular fragmentation.

TABLE OF CONTENTS

	Page
LIST OF TABLES	vii
LIST OF FIGURES	viii
1 Introduction	1
1.1 Coulomb Explosion	1
1.2 Hydrocarbons	1
1.3 Theoretical Models	1
1.4 Research Objectives and Approach	2
2 Computational Method	3
3 Results	6
3.1 Laser Parameters and Intensity Optimization	6
3.2 Methane (CH_4)	7
3.2.1 Dynamics	7
3.2.2 Distribution	8
3.3 Ethane (C_2H_6)	9
3.3.1 Dynamics	9
3.3.2 Distribution	11
3.4 Propane (C_3H_8)	12
3.4.1 Dynamics	12
3.4.2 Distribution	12
3.5 Butane (C_4H_{10})	13
3.5.1 Dynamics	13
3.5.2 Distribution	13
4 Summary	16
References	18

LIST OF TABLES

Table	Page
3.1 Approximate pulse intensities required for ionization, fragmentation, and dissociation of the first four alkanes.	6

LIST OF FIGURES

Figure	Page
3.1 CH ₄ Coulomb explosion snapshots resulting in the formation of one CH ₂ molecule and two discharged H atoms have 1.26 ⁺ , 0.62 ⁺ , and 0.84 ⁺ charges, respectively (the 0.5, 0.1, 0.01, and 0.001 density isosurfaces are displayed). The pulse electric field and the number of electrons in the simulation are shown, with vertical dashed purple lines indicating the specific times in the simulation when each snapshot was captured.	7
3.2 Average production frequency of each fragment generated in 71 CH ₄ Coulomb explosion simulations. The darker columns represent the formation frequency of hydrogen fragments and carbon-containing fragments. The lighter appended columns indicate the corresponding average charges associated with each produced fragment	8
3.3 Snapshots of the Coulomb explosion of C ₂ H ₆ , illustrating the formation of CH ₂ and CH ₃ fragments, which carry charges of 1.18 ⁺ and 1.18 ⁺ , respectively (the 0.5, 0.1, 0.01, and 0.001 density isosurfaces are shown). The bar between the two fragments at 120 fs denotes the distance between their center of masses.	9
3.4 Distance (top) and speed (bottom) between the CH ₂ and CH ₃ shown in Figure 3.3 from 120 fs to 500 fs. Note that 1Å/fs is 100000 m/s.	10
3.5 Histogram illustrating the average production frequency and charge of each fragment generated in 50 C ₂ H ₆ Coulomb explosion simulations.	11
3.6 C ₃ H ₈ Coulomb explosion snapshots resulting in the formation of C ₂ H and CH ₂ fragments with 2.22 ⁺ and 0.91 ⁺ charges, respectively (the 0.5, 0.1, 0.01, and 0.001 density isosurfaces are shown). The bar between the two fragments at 120 fs denotes the distance between their center of masses.	12
3.7 Histogram illustrating the average production frequency and charge of each fragment generated in 50 C ₃ H ₈ Coulomb explosion simulations.	13
3.8 C ₄ H ₁₀ Coulomb explosion snapshots resulting in the formation of C ₂ H ₂ and two CH ₂ fragments measured to have 1.12 ⁺ , 0.77 ⁺ and 0.90 ⁺ charges, respectively (the 0.5, 0.1, 0.01, and 0.001 density isosurfaces are shown).	14
3.9 Histogram illustrating the average production frequency and charge of each fragment generated in 88 C ₄ H ₁₀ Coulomb explosion simulations.	14

CHAPTER 1

Introduction

1.1 Coulomb Explosion

Recent advancements in ultrafast, high-intensity laser technology have enabled real-time studies of electron and ion dynamics in extreme environments with unprecedented temporal resolution [1–3]. This progress has facilitated extensive investigations into Coulomb explosion—a phenomenon in which a laser ionizes a molecule, causing the remaining positively charged ions to repel each other. The Coulomb explosion process not only provides insights into the behavior of atoms in these high-energy environments [3], but also has diverse applications, including molecular imaging [4–29], structural dynamics [30–41], the generation of bright keV x-ray photons [42, 43], the production of high-energy electrons [44], and nuclear energy [45–52]. As a result of these diverse applications, laser-pulse-driven molecular fragmentation has emerged as a central focus of extensive research efforts [39, 53–64].

1.2 Hydrocarbons

Hydrocarbon molecules such as methane, ethane, propane, and butane are commonly used precursors in Coulomb explosion studies [46, 64–69] due to their ubiquity in natural [70] and astrophysical environments [71, 72]. These investigations have highlighted several critical observations, including proton kinetic energies, plasma emission spectra, and fragment yields over various pulse intensities. Despite this progress, a detailed dynamical understanding of the fragmentation process remains elusive. Specifically, there is a lack of systematic studies identifying optimal laser pulse parameters and intensities to maximize fragmentation efficiency in the first four alkanes and the products distributions that are yielded from the explosion.

1.3 Theoretical Models

Theoretical models of Coulomb explosion have evolved over time, ranging from classical approaches that omit quantum effects [25–29, 56, 73–83], to semiclassical methods [9, 84], and *ab initio* techniques [85–91]. Classical models assume purely repulsive interactions between positively charged atomic cores, neglecting the attractive forces arising from electron densities. In contrast, *ab initio* methods like time-dependent density functional theory (TDDFT) [92, 93] incorporate these interactions, enabling the simulation of bonded fragment formation. Due to TDDFT’s demonstrated accuracy in reproducing experimental results [87–91], it serves as the foundation for this study.

1.4 Research Objectives and Approach

In this work, TDDFT simulations are employed to explore the fragmentation dynamics of hydrocarbons under Coulomb explosion induced by intense laser fields. This study is motivated by recent experiments that observed CH radicals and other fragments resulting from the Coulomb explosion of ethene [94] and butane [95]. The results are somewhat surprising, as earlier experiments [32, 91] primarily demonstrated that strong laser pulses predominantly stripped protons from hydrocarbon molecules via a CH bond stretching mechanism. This study analyzes fragment charge distributions, electron dynamics during ionization, and post-ionization molecular motion, identifying laser intensities that optimize fragmentation.

By focusing on methane, ethane, propane, and butane, this research uncovers fragmentation behaviors unique to their molecular structures and ionization potentials. The findings contribute to a deeper understanding of Coulomb explosion mechanisms and offer valuable insights for designing future experiments.

CHAPTER 2

Computational Method

The simulations were performed using TDDFT for modeling the electron dynamics on a real-space grid with real-time propagation [96], with the Kohn-Sham (KS) Hamiltonian of the following form

$$\hat{H}_{\text{KS}}(t) = -\frac{\hbar^2}{2m}\nabla^2 + V_{\text{ion}}(\mathbf{r}, t) + V_{\text{H}}[\rho](\mathbf{r}, t) + V_{\text{XC}}[\rho](\mathbf{r}, t) + V_{\text{laser}}(\mathbf{r}, t). \quad (2.1)$$

Here, ρ is the electron density which is defined as the density sum over all occupied orbitals:

$$\rho(\mathbf{r}, t) = \sum_{k=1}^{N_{\text{orbitals}}} 2|\psi_k(\mathbf{r}, t)|^2, \quad (2.2)$$

where the coefficient 2 accounts for there being two electrons in each orbital (via spin degeneracy) and k is a quantum number labeling each orbital.

V_{ion} in Eq. (2.1) is the external potential due to the ions, represented by employing norm-conserving pseudopotentials centered at each ion as given by Troullier and Martins [97]. V_{H} is the Hartree potential, defined as

$$V_{\text{H}}(\mathbf{r}, t) = \int \frac{\rho(\mathbf{r}', t)}{|\mathbf{r} - \mathbf{r}'|} d\mathbf{r}', \quad (2.3)$$

and accounts for the electrostatic Coulomb interactions between electrons. The term V_{XC} is the exchange-correlation potential, which is approximated by the adiabatic local-density approximation (ALDA), obtained from a parameterization to a homogeneous electron gas by Perdew and Zunger [98]. The last term in Eq. (2.1), V_{laser} is the time-dependent potential due to the electric field of the laser, and is described using the dipole approximation, $V_{\text{laser}} = \mathbf{r} \cdot \mathbf{E}_{\text{laser}}(t)$. The electric field $\mathbf{E}_{\text{laser}}(t)$ is given by

$$\mathbf{E}_{\text{laser}}(t) = E_{\text{max}} \exp\left[-\frac{(t - t_0)^2}{2a^2}\right] \sin(\omega t) \hat{\mathbf{k}}, \quad (2.4)$$

where the parameters E_{max} , t_0 , and a define the maximum amplitude, initial position of the center, and the width of the Gaussian envelope, respectively. ω describes the frequency of the laser and $\hat{\mathbf{k}}$ is the unit vector in the polarization direction of the electric field.

At the beginning of the TDDFT calculations, the ground state of the system is prepared by performing a Density-Functional Theory (DFT) calculation. With these initial conditions in place, the Kohn-Sham orbitals,

$\psi_k(\mathbf{r}, t)$, are then propagated over time using the time-dependent KS equation, given as

$$i \frac{\partial \psi_k(\mathbf{r}, t)}{\partial t} = \hat{H} \psi_k(\mathbf{r}, t). \quad (2.5)$$

Eq. (2.5) was solved using the following time propagator

$$\psi_k(\mathbf{r}, t + \delta t) = \exp\left(-\frac{i\hat{H}_{\text{KS}}(t)\delta t}{\hbar}\right) \psi_k(\mathbf{r}, t). \quad (2.6)$$

This operator is approximated using a fourth-degree Taylor expansion, given as

$$\psi_k(\mathbf{r}, t + \delta t) \approx \sum_{n=0}^4 \frac{1}{n!} \left(\frac{-i\delta t}{\hbar} \hat{H}_{\text{KS}}(t) \right)^n \psi_k(\mathbf{r}, t). \quad (2.7)$$

The operator is applied for N time steps until the final time, $t_{\text{final}} = N \cdot \delta t$, is obtained. A time step of $\delta t = 1$ as was used in the simulations.

In real-space TDDFT, the Kohn-Sham orbitals are represented at discrete points in real space. These points are organized on a uniform rectangular grid. The accuracy of the simulations is determined by the grid spacing, which is the key parameter that can be adjusted. In the simulations, a grid spacing of 0.3 Å was used with 100 points placed along each of the x , y , and z axes.

To enforce boundary conditions, the Kohn-Sham orbitals were set to zero at the edges of the simulation cell. However, when a strong laser field is applied, ionization can occur, potentially causing unphysical reflections of the wavefunction at the cell boundaries. To address this issue, a complex absorbing potential (CAP) was implemented to dampen the wavefunction as it reaches the boundaries. The specific form of the CAP used in the simulations, as described by Manopoulous [99], is given by:

$$-iw(x) = -i \frac{\hbar^2}{2m} \left(\frac{2\pi}{\Delta x} \right)^2 f(y), \quad (2.8)$$

where x_1 is the start and x_2 is the end of the absorbing region, $\Delta x = x_2 - x_1$, $c = 2.62$ is a numerical constant, m is the electron's mass, and

$$f(y) = \frac{4}{c^2} \left(\frac{1}{(1+y)^2} + \frac{1}{(1-y)^2} - 2 \right), \quad y = \frac{x-x_1}{\Delta x}. \quad (2.9)$$

As the molecule is ionized by the laser field, the electron density is directed towards the CAP. Additionally, the ejected fragments carry their electron density move towards the CAP. When any electron density into

contact with the CAP, it is absorbed. Consequently, the total electron number

$$N(t) = \int_V \rho(\mathbf{r}, t) d^3x, \quad (2.10)$$

where V is the volume of the simulation box, will diverge from the initial electron number, $N(0)$. $N(0) - N(t)$ is interpreted as the total number of electrons ejected from the simulation box.

Motion of the ions in the simulations were treated classically. Using the Ehrenfest theorem, the quantum forces on the ions due to the electrons are given by the derivatives of the expectation value of the total electronic energy with respect to the ionic positions. These forces are then fed into Newton's Second Law, giving

$$M_i \frac{d^2\mathbf{R}_i}{dt^2} = Z_i \mathbf{E}_{\text{laser}}(t) + \sum_{j \neq i}^{N_{\text{ions}}} \frac{Z_i Z_j (\mathbf{R}_i - \mathbf{R}_j)}{|\mathbf{R}_i - \mathbf{R}_j|^3} - \nabla_{\mathbf{R}_i} \int V_{\text{ion}}(\mathbf{r}, \mathbf{R}_i) \rho(\mathbf{r}, t) d\mathbf{r}, \quad (2.11)$$

where M_i , Z_i , and \mathbf{R}_i are the mass, pseudocharge (valence), and position of the i -th ion, respectively, and N_{ions} is the total number of ions. This differential equation was time propagated using the Verlet algorithm at every time step δt . This approach has been successfully used to describe the Coulomb explosion of molecules [87–91].

In each simulation, the ion velocities are initialized using a Boltzmann distribution corresponding to 300 K. This random initialization facilitates the exploration of various fragmentation pathways during the Coulomb explosion. If the ion velocities were held constant, the simulations would yield identical fragmentation outcomes, thus constraining the statistical variability of the results. To ensure a comprehensive distribution of data, more than 50 simulations were conducted for each molecule, allowing for the formation of $C_n H_m$ fragments in several instances across all tested molecules. Due to limited computational resources, no further simulations were performed.

Each molecule in the simulations was positioned at the center of the simulation box, with its longest molecular axis aligned along the x -axis and its shortest axis oriented along the z -axis. In every simulation, the electric field was polarized along the x -axis to maximize ionization [87]. These conditions model experiment, where precise molecular alignment is achievable [5].

The following section presents the results from a substantial number of simulations conducted on the first four alkanes: methane (CH_4), ethane (C_2H_6), propane (C_3H_8), and butane (C_4H_{10}), using a laser intensity determined to optimize fragmentation. The laser parameters, including wavelength and duration, were modeled after the pulse described in [95], which follows the functional form outlined in Eq. (2.4). The only varying parameter in the simulations was the laser intensity, which was adjusted to explore the ionization, fragmentation, and dissociation ranges for the selected alkanes.

CHAPTER 3

Results

3.1 Laser Parameters and Intensity Optimization

The optimal laser intensities for fragmentation that were used in the simulations are presented in Table 3.1. All simulations employed a pulse wavelength of 890 nm and a duration of 7.8 fs (FWHM), with intensity being the only variable parameter. The results highlight three distinct regimes of laser intensity: (1) intensities below the ionization threshold, which result in minimal dissociation, (2) intensities near the fragmentation threshold, which produce partial breakup and smaller ionized fragments, and (3) intensities exceeding the dissociation threshold, resulting in complete molecular breakup driven by strong Coulomb repulsion between the ions.

For CH₄, an intensity of 1.1×10^{15} W/cm² was optimal for producing the richest diversity of fragmentation pathways (see Table 3.1). Lower intensities, such as 7×10^{14} W/cm², led to ionization without significant fragmentation, while higher intensities, exceeding 1.5×10^{15} W/cm², caused complete molecular dissociation. Intermediate laser intensities, ranging from the ionization to the dissociation thresholds, were also explored. At intensities between the fragmentation and dissociation threshold, smaller fragments, such as C and CH, were observed with little diversity. At intensities between the ionization and fragmentation threshold, fragmentation was less effective, often leading to partial dissociation and the formation of larger fragments, such as CH₃.

The same technique was applied for the other three alkanes. For C₂H₆, a pulse intensity of 9.0×10^{14} W/cm² produced the most diverse fragmentation products. Similarly, an intensity of 7×10^{14} W/cm² was optimal for C₃H₈ and C₄H₁₀ (see Table 3.1). For all molecules, lower intensities produced incomplete dissociation or larger fragments, whereas higher intensities led to excessive dissociation into individual ions

Alkane	Ionization threshold (W/cm ²)	Fragmentation threshold (W/cm ²)	Dissociation threshold (W/cm ²)
CH ₄	7.0×10^{14}	1.1×10^{15}	1.5×10^{15}
C ₂ H ₆	6.1×10^{14}	9.0×10^{14}	1.5×10^{15}
C ₃ H ₈	3.8×10^{14}	7.0×10^{14}	1.5×10^{15}
C ₄ H ₁₀	4.5×10^{14}	7.0×10^{14}	1.3×10^{15}

Table 3.1: Approximate pulse intensities required for ionization, fragmentation, and dissociation of the first four alkanes.

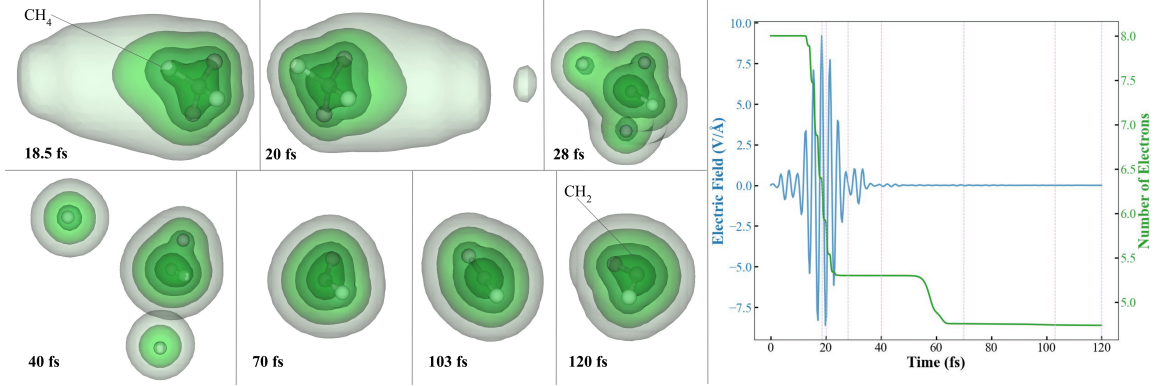


Figure 3.1: CH_4 Coulomb explosion snapshots resulting in the formation of one CH_2 molecule and two discharged H atoms have 1.26^+ , 0.62^+ , and 0.84^+ charges, respectively (the 0.5, 0.1, 0.01, and 0.001 density isosurfaces are displayed). The pulse electric field and the number of electrons in the simulation are shown, with vertical dashed purple lines indicating the specific times in the simulation when each snapshot was captured.

without bonding.

It is important to note that in experimental setups, only a fraction of the molecular target is exposed to the laser pulse's peak intensity. Molecules outside the focal region interact with lower-intensity fields, resulting in a range of fragmentation pathways occurring simultaneously.

In the following sections, simulations were performed using laser intensities at the fragmentation thresholds listed in Table 3.1. These intensities were selected because they produce diverse fragmentation pathways, allowing for a detailed analysis of the fragmentation dynamics and distributions of each hydrocarbon.

3.2 Methane (CH_4)

3.2.1 Dynamics

The electron densities and molecular dynamics of a CH_4 molecule during a Coulomb explosion simulation are illustrated in Figure 3.1. These snapshots are from one of the 71 simulations conducted using CH_4 as the precursor molecule. Initially, the snapshots show how the laser field rips the electron density away from the molecule, triggering rapid ionization. As shown in the figure, significant ionization begins when the electric field magnitude reaches approximately $5.5 \text{ V}/\text{\AA}$ at 14 fs. The ionization process concludes when the laser field falls below $6 \text{ V}/\text{\AA}$ at around 24 fs, leaving the molecule with 5.3 valence electrons. This near-triple ionization creates strong Coulomb repulsion between the resulting fragments, causing them to separate rapidly. In the calculations, the electron density is integrated over a finite volume, resulting in non-integer electron counts. This phenomenon can be interpreted in several ways. One interpretation suggests that approximately 5.3 electrons remain localized within the molecular region during the simulation, with the fractional charge either recombining with the ionized electron cloud or dissociating over a longer simulation

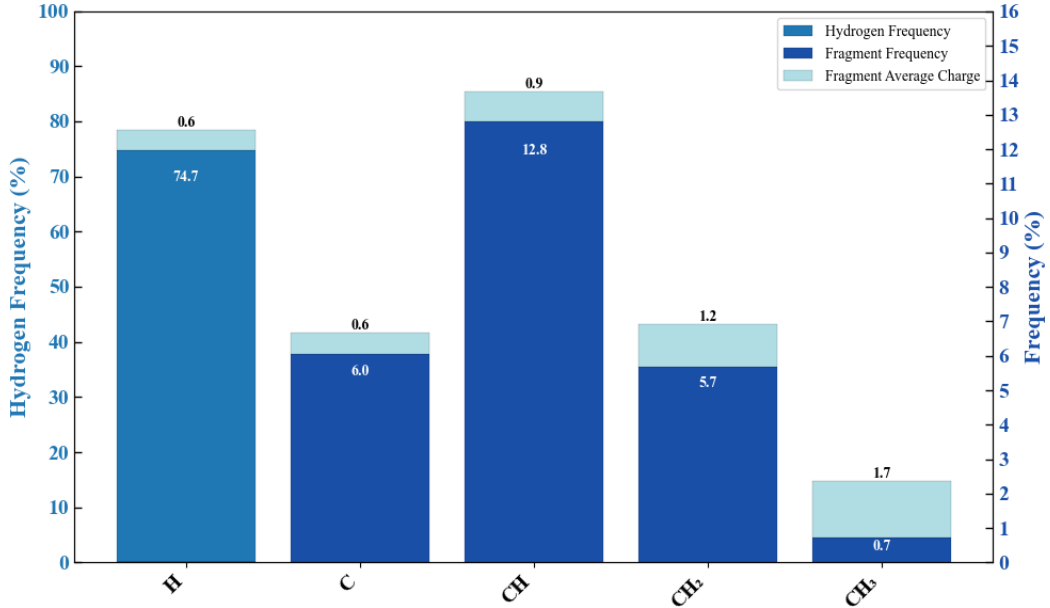


Figure 3.2: Average production frequency of each fragment generated in 71 CH_4 Coulomb explosion simulations. The darker columns represent the formation frequency of hydrogen fragments and carbon-containing fragments. The lighter appended columns indicate the corresponding average charges associated with each produced fragment

period. Alternatively, the non-integer charge could be understood as an average, where some molecular fragments retain 5 valence electrons, others 6, and 5.3 represents the mean electron count per fragment. For example, if a hydrogen atom was ejected with a charge of 0.6^+ , that would indicate that 60% of the time it would be detected as a 1^+ ion, and 40% of the time it would be a neutral hydrogen atom.

Following ionization, the remaining fragment (CH_2) undergoes structural rearrangement. Figure 3.1 depicts the CH_2 fragment transitioning from a right-bent geometry at 70 fs to a linear conformation at 103 fs, and finally to a left-bent structure at 120 fs. Additionally, the ejected hydrogen fragments are observed moving toward the CAP, where their electrons are absorbed. This process results in a further (artificial) reduction in the number of electrons, as shown by the drop in electron count around 50 fs in Figure 3.1.

3.2.2 Distribution

Figure 3.2 illustrates the distribution of fragments and their corresponding charges resulting from the Coulomb explosion of CH_4 . The data demonstrate that the reaction yields a range of hydrocarbons smaller than CH_4 . Among these fragments, CH is the most frequently observed carbon-containing species, appearing in 12.8% of the simulations with an average charge of 0.9^+ . Hydrogen fragments are the most commonly detected overall, with an average charge of 0.6^+ (equivalent to 0.4 electrons) as they approach the CAP. Other fragments, such as CH_2 and CH_3 , are also present but occur less frequently. Importantly, no CH_4 fragments

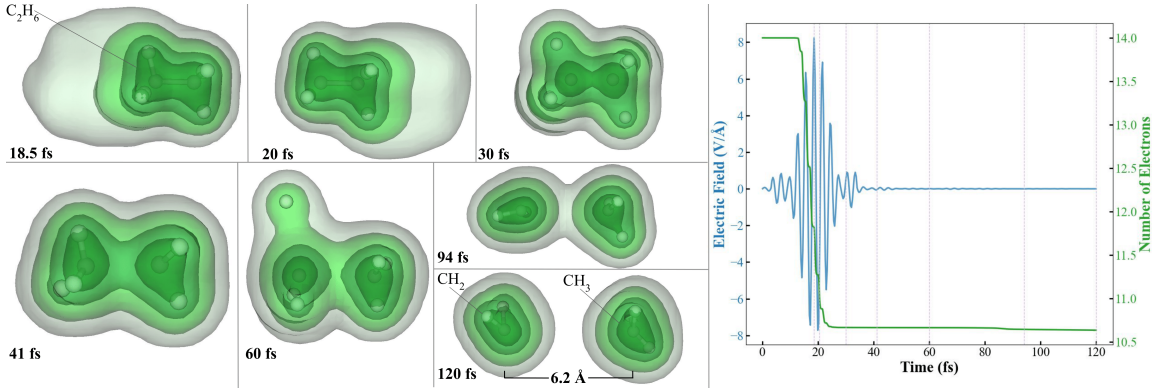


Figure 3.3: Snapshots of the Coulomb explosion of C₂H₆, illustrating the formation of CH₂ and CH₃ fragments, which carry charges of 1.18⁺ and 1.18⁺, respectively (the 0.5, 0.1, 0.01, and 0.001 density isosurfaces are shown). The bar between the two fragments at 120 fs denotes the distance between their center of masses.

were observed, indicating that the laser pulse intensity was sufficiently strong to dissociate at least one atom from the molecule in every simulation. On average, the laser ejected 2.72 electrons per simulation. These simulations help determine the optimal pulse parameters and predict the dissociation pathways for CH₄ in Coulomb explosion fragmentation.

3.3 Ethane (C₂H₆)

3.3.1 Dynamics

Figure 3.3 presents snapshots from one of the 50 Coulomb explosion simulations with C₂H₆ as the precursor molecule. These snapshots illustrate the interaction between the electric field of the laser pulse and the electron density of the molecule. The field stretches and compresses the electron density. As shown in the pulse diagram in Figure 3.3, when the electric field exceeds 5 V/Å, between 14 fs and 22 fs, rapid ionization occurs, reducing the valence electron count to approximately 10.7. Following the dissipation of the laser pulse at 40 fs, two CH₃ fragments are produced. By 60 fs, due to the asymmetric charge distribution, one of the fragments ejects a hydrogen atom. The ionization induces strong Coulomb repulsion between the resulting fragments, causing the CH₂ and CH₃ groups to visibly repel each other throughout the simulation. Additionally, the snapshots reveal rotational motion of the fragments, particularly within the CH₂ fragment. Between 60 and 94 fs, the CH₂ molecule rotates approximately 90 degrees about the *z*-axis, followed by an additional 90-degree rotation from 94 to 120 fs.

The CH₂⁺ and CH₃⁺ fragments are well separated at the end of the TDDFT simulation in Figure 3.3. Figure 3.4 shows how the fragments move after 120 fs assuming that the two charged fragments interact via the Coulomb potential and their motion can be described by solving the Newton equations of motions using the Verlet algorithm. By the conclusion of the TDDFT simulation, the centers of mass of the molecules

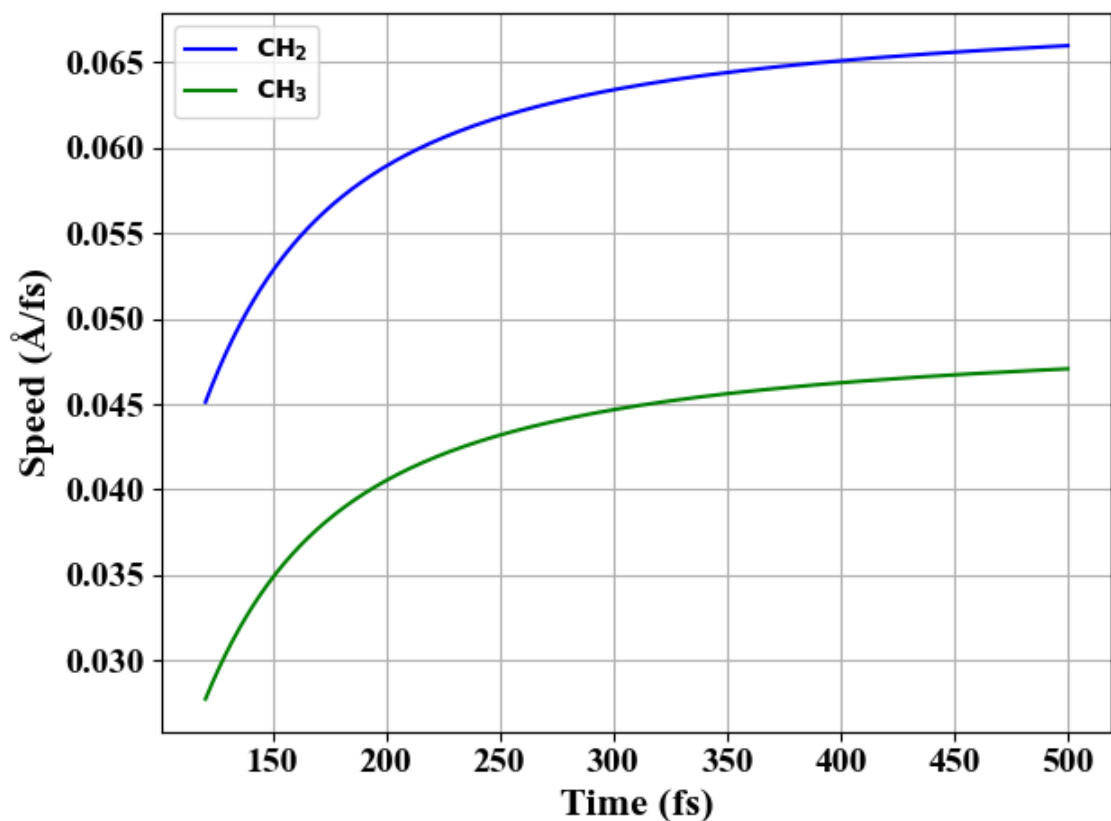
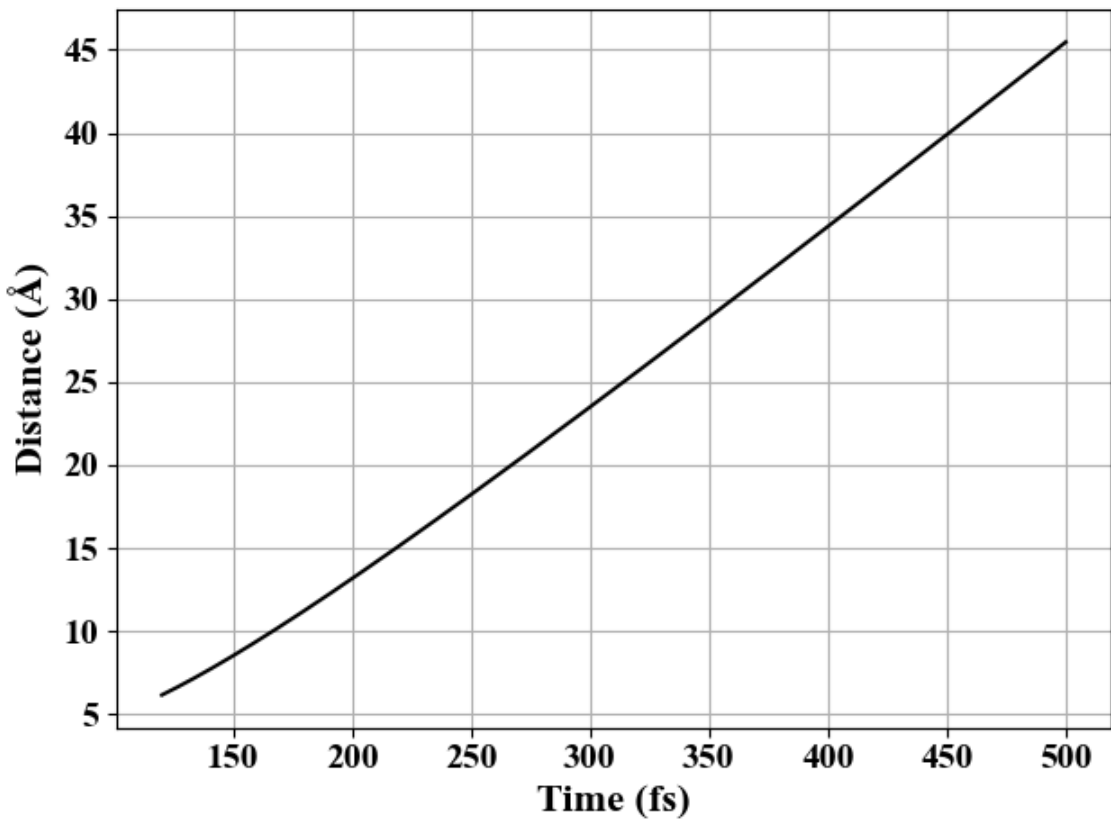


Figure 3.4: Distance (top) and speed (bottom) between the CH₂ and CH₃ shown in Figure 3.3 from 120 fs to 500 fs. Note that 1 $\text{\AA}/\text{fs}$ is 100000 m/s.

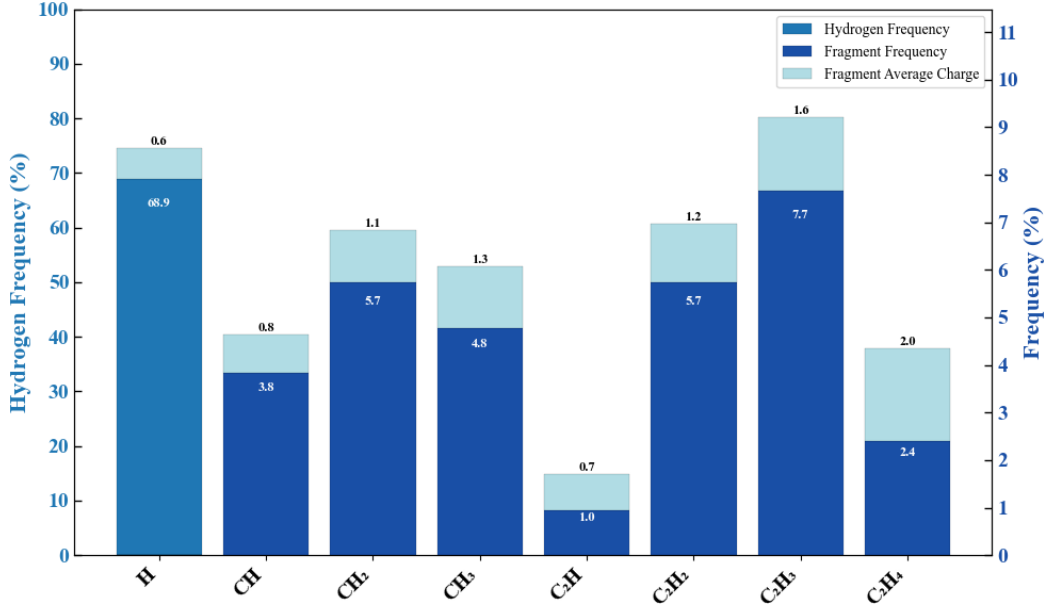


Figure 3.5: Histogram illustrating the average production frequency and charge of each fragment generated in 50 C₂H₆ Coulomb explosion simulations.

were separated by 6.2 Å. Figure 3.4 shows that the acceleration gradually decreases and the distance between the ions grows linearly. At 500 fs, the distance between the molecules increased to 45 Å, with the CH₂⁺ and CH₃⁺ groups each exhibiting velocities of 6.6×10^{-2} Å/fs (6600 m/s) and 4.7×10^{-2} Å/fs (4700 m/s), respectively. The large difference in velocity is due to the difference between the initial velocities of the fragments. In experiment, the velocity of the CH₂⁺ ion in Coulomb explosion of methanol has been measured to be 4800 m/s [57], which is within the same magnitude as in the present calculations. Considering that the laser intensity used in the simulations is six times higher than in the experiment, this agreement is remarkably good.

3.3.2 Distribution

Figure 3.5 shows the distribution of fragments and their corresponding charges resulting from the Coulomb explosion of C₂H₆. The data reveal that the fragmentation produces various hydrocarbons smaller than C₂H₆. Among these fragments, C₂H₃ is the most frequently detected carbon-containing species, appearing in 7.7% of the simulations with an average charge of 1.6⁺. Hydrogen fragments are the most prevalent overall, carrying an average charge of 0.6⁺ as they are ejected from the molecule. Other fragments, including CH, CH₂, and C₂H₃, are also observed but with lower frequencies. Notably, no C₂H₆ or C₂H₅ fragments were detected, indicating that the laser pulse intensity was sufficient to dissociate at least two hydrogen atoms from the molecule in every simulation. On average, the laser ejected 3.42 electrons per simulation.

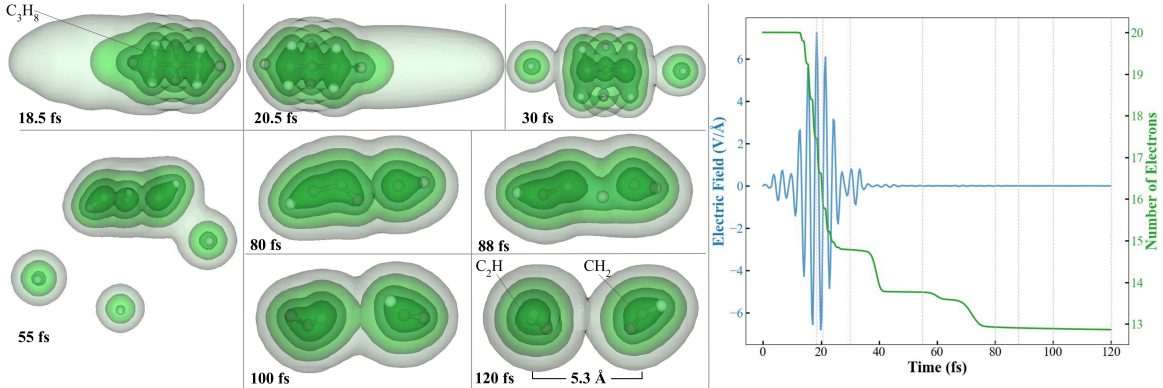


Figure 3.6: C_3H_8 Coulomb explosion snapshots resulting in the formation of C_2H and CH_2 fragments with 2.22^+ and 0.91^+ charges, respectively (the 0.5, 0.1, 0.01, and 0.001 density isosurfaces are shown). The bar between the two fragments at 120 fs denotes the distance between their center of masses.

3.4 Propane (C_3H_8)

3.4.1 Dynamics

Figure 3.6 shows snapshots from one of the 50 Coulomb explosion simulations using C_3H_8 as the precursor molecule. These images depict how the laser pulse's electric field interacts with the molecule's electron density, stretching it and expelling it from the molecule, which leads to fragmentation. According to the pulse diagram in Figure 3.6, rapid ionization occurs when the electric field intensity exceeds $4 \text{ V}/\text{\AA}$ from approximately 14 fs to 24 fs, resulting in the retention of 14.8 valence electrons in the molecule. This ionization leads to the ejection of two hydrogen atoms at 30 fs, followed by the ejection of three additional hydrogen atoms at 55 fs. At 88 fs in the simulation, a hydrogen atom is observed transferring from the C_2H fragment to the CH fragment, indicating that molecular rearrangement and bonding can occur even after the laser-induced ionization. As illustrated in the figure, the resulting Coulomb explosion and subsequent molecular dynamics lead to the formation of C_2H and CH_2 fragments.

3.4.2 Distribution

Figure 3.7 presents the distribution of fragments and their corresponding charges resulting from the Coulomb explosion of C_3H_8 . The data reveals the diverse set of fragmentation pathways achievable with C_3H_8 as the precursor molecule, among which C_3H is the most commonly observed hydrocarbon, appearing in 2.8% of the simulations with an average charge of 1.2^+ . Hydrogen fragments are the most frequently detected overall, exhibiting an average charge of 0.6^+ as they near the CAP. Other fragments, such as CH , C_3 , and C_3H , are also present but with a lower formation rate. Importantly, no fragments of C_3H_4 or larger were found, suggesting that the laser pulse intensity was adequate to remove at least five hydrogen atoms from the molecule in each simulation. On average, the laser expelled 5.15 electrons per simulation.

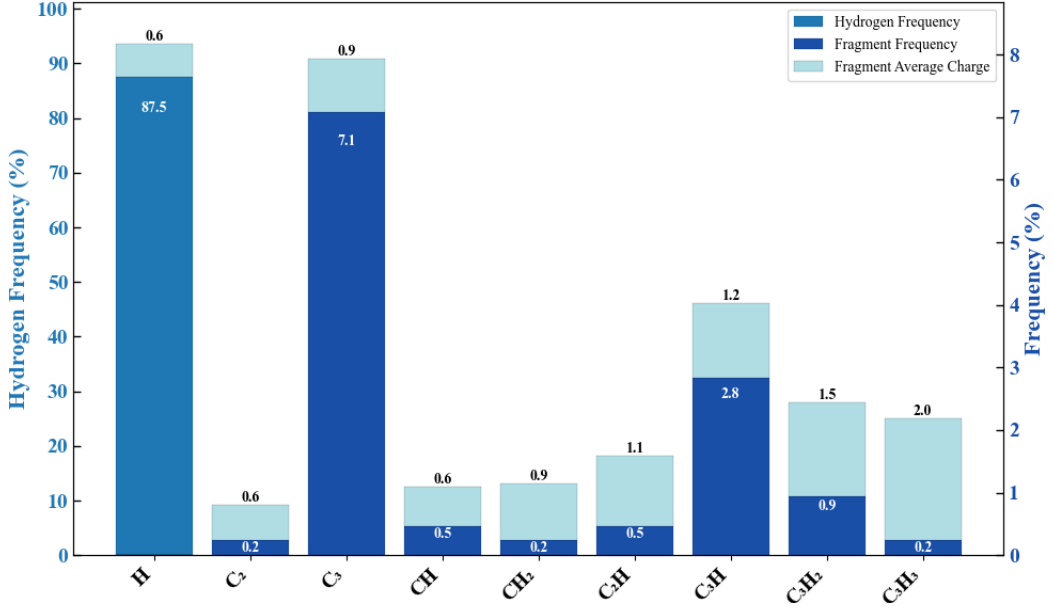


Figure 3.7: Histogram illustrating the average production frequency and charge of each fragment generated in 50 C_3H_8 Coulomb explosion simulations.

3.5 Butane (C_4H_{10})

3.5.1 Dynamics

Figure 3.8 shows snapshots from one of the 88 Coulomb explosion simulations conducted with C_4H_{10} in the gauche conformation the precursor molecule. These snapshots capture the dynamic interaction between the laser pulse's electric field and the electron density of the molecule, which causes the electron density to stretch and be expelled toward the CAP. As illustrated in the pulse diagram in Figure 3.8, when the electric field intensity surpasses 4 V/ \AA (between 14 fs and 24 fs), a rapid ionization process occurs, leaving 20.5 valence electrons in the molecule. Similarly to the previous case, by the end of the laser pulse at approximately 30 fs, two hydrogen atoms are ejected. Additionally, the CH bond involving the two hydrogen atoms at the top is significantly stretched, resulting in further ejection around 45 fs. In this instance, the system ultimately forms a charged C_2H_2 molecule along with two charged CH_2 fragments.

3.5.2 Distribution

Figure 3.9 displays the distribution and charges of fragments resulting from the Coulomb explosion of C_4H_{10} . The data indicate a diverse range of fragmentation products. Among these, CH_2 is the most frequently observed hydrocarbon, appearing in 6.8% of the simulations with an average charge of 0.9^+ . Hydrogen fragments are the most prevalent overall, exhibiting an average charge of 0.6^+ as they approach the CAP. Other fragments such as CH, CH_2 , and C_2H_2 are also present but occur less frequently. The laser pulse

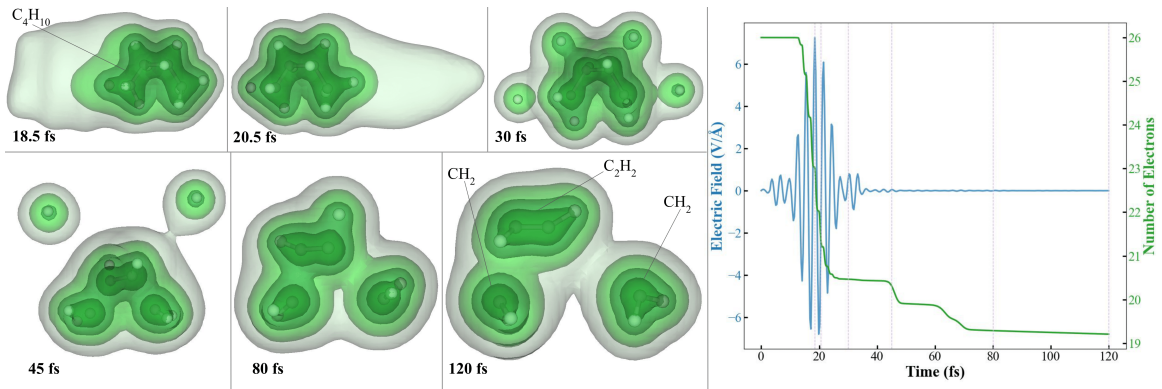
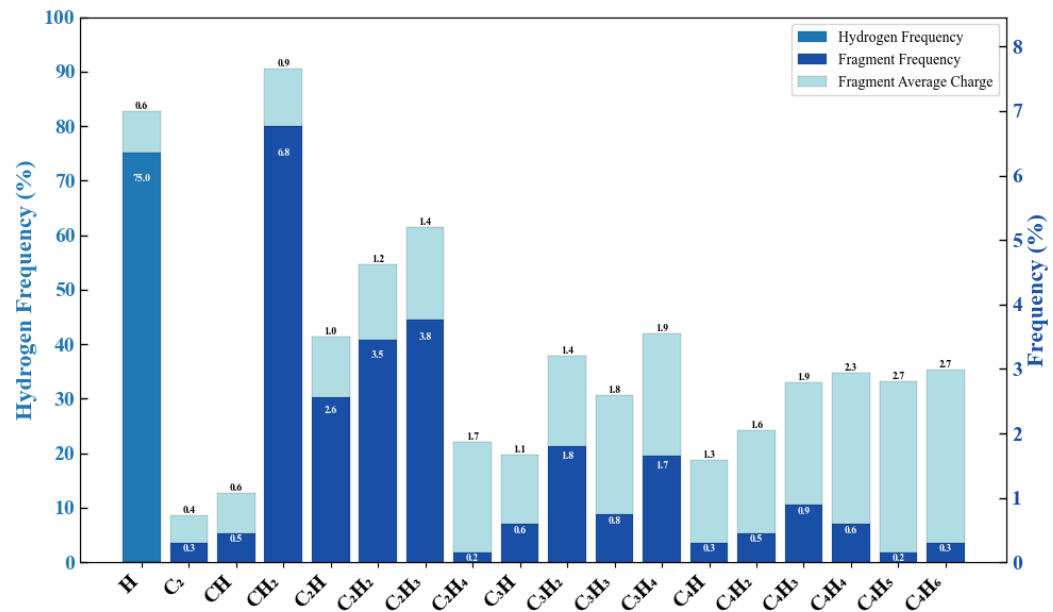


Figure 3.8: C_4H_{10} Coulomb explosion snapshots resulting in the formation of C_2H_2 and two CH_2 fragments measured to have 1.12^+ , 0.77^+ and 0.90^+ charges, respectively (the 0.5, 0.1, 0.01, and 0.001 density isosurfaces are shown).



intensity was sufficient to remove at least three hydrogen atoms from the molecule in each simulation, as no fragments larger than C₃H₆ were detected. On average, the laser ejected 5.54 electrons per simulation. These results are crucial for optimizing pulse parameters and predicting the fragmentation pathways of C₄H₁₀ in Coulomb explosion studies.

CHAPTER 4

Summary

Fragmentation in the Coulomb explosion of hydrocarbon molecules was investigated using time-dependent density-functional theory simulations. This approach enables the visualization of the underlying mechanisms of fragment formation, the prediction of product formation pathways, and the identification of ideal intensities for diverse fragmentation. It has been demonstrated that at specific regions of laser intensity, hydrocarbon molecules dissociate into charged fragments consisting of n carbon and m hydrogen atoms, denoted as C_nH_m . Higher laser intensities result in the complete dissociation of the molecule, while lower intensities typically lead to the stripping of protons or cause only ionization (refer to Table 3.1). The C_nH_m fragments can be experimentally detected [95].

The optimal pulse intensities that yielded the most favorable fragmentation distributions for CH_4 , C_2H_6 , C_3H_8 , and C_4H_{10} were determined to be $1.1 \times 10^{15} \text{ W/cm}^2$, $9 \times 10^{14} \text{ W/cm}^2$, $7 \times 10^{14} \text{ W/cm}^2$, and $7 \times 10^{14} \text{ W/cm}^2$, respectively (as demonstrated in Table 3.1). All other laser parameters, including wavelength, duration, and center frequency, were held constant for each molecule across their respective simulations. The electric field strength—and consequently, the intensity—was the only parameter adjusted for each molecule.

Notably, ionization of the molecule in each simulation occurred only when the laser electric field exceeded a specific range corresponding to each molecule. Fig. 3.1, Fig. 3.3, Fig. 3.6, and Fig. 3.8 illustrate the electric field of the laser and the number of electrons in the molecule over time, demonstrating that ionization occurs approximately 5 fs before and after the peak electric field.

The initialization of velocities based on the Boltzmann distribution at 300 K facilitated the distribution of fragment products for each molecule using the same laser pulse across all simulations. The statistical distributions of fragment production frequencies provide crucial insights into predicting the probabilities of various fragment formation pathways for each tested molecule. Furthermore, the average charge of the fragments indicates the likelihood of different charge states for a molecule. Fig. 3.9, for example, depicts an average charge of 0.6^+ for the produced CH species, which suggests that any CH fragment resulting from the Coulomb explosion has a 60% probability of being positively charged and a 40% probability of being neutral.

Moreover, a comparison of the histograms for all molecules (Fig. 3.2, Fig. 3.5, Fig. 3.7, Fig. 3.9) provides valuable insights. For instance, the average charge of the expelled free hydrogen is consistently 0.6^+ across all precursor molecules. Notable similarities are observed in the characteristics of the CH fragments as well. The two smaller alkanes (CH_4 and C_2H_6) produced CH fragments with an average charge of 0.8^+ , while the two larger alkanes (C_3H_8 and C_4H_{10}) yielded CH fragments with an average charge of 0.6^+ .

The snapshot diagrams from specific simulations illustrate the formation of fragments and bonds following the rapid ionization induced by a strong laser field. These images provide crucial insights into the discharge of electron density from the molecule and the repulsion between the resulting charged fragments. Additionally, the snapshots enable the study of fragment dynamics after the laser-driven ionization, including structural rearrangements (Fig. 3.1), rotations (Fig. 3.3), and the transfer of atoms between different fragments (Fig. 3.6).

Future work could involve experimental validation of these findings to refine theoretical models, particularly by exploring different laser parameters and molecular environments. Such experimental efforts will help bridge the gap between theory and practice, providing a more comprehensive understanding of fragmentation dynamics of the Coulomb explosion.

References

- [1] Ursula Keller. Recent developments in compact ultrafast lasers. *Nature*, 424(6950):831–838, Aug 2003. ISSN 1476-4687. doi: 10.1038/nature01938. URL <https://doi.org/10.1038/nature01938>.
- [2] Ferenc Krausz and Misha Ivanov. Attosecond physics. *Rev. Mod. Phys.*, 81:163–234, Feb 2009. doi: 10.1103/RevModPhys.81.163. URL <https://link.aps.org/doi/10.1103/RevModPhys.81.163>.
- [3] Alicia Palacios and Fernando Martín. The quantum chemistry of attosecond molecular science. *WIREs Computational Molecular Science*, 10(1):e1430, 2020. doi: <https://doi.org/10.1002/wcms.1430>. URL <https://wires.onlinelibrary.wiley.com/doi/abs/10.1002/wcms.1430>.
- [4] Z. Vager, R. Naaman, and E. P. Kanter. Coulomb explosion imaging of small molecules. *Science*, 244(4903):426–431, 1989. doi: 10.1126/science.244.4903.426. URL <https://www.science.org/doi/abs/10.1126/science.244.4903.426>.
- [5] Constant A. Schouder, Adam S. Chatterley, James D. Pickering, and Henrik Stapelfeldt. Laser-induced coulomb explosion imaging of aligned molecules and molecular dimers. *Annual Review of Physical Chemistry*, 73(Volume 73, 2022):323–347, 2022. ISSN 1545-1593. doi: <https://doi.org/10.1146/annurev-physchem-090419-053627>. URL <https://www.annualreviews.org/content/journals/10.1146/annurev-physchem-090419-053627>.
- [6] Philipp Herwig, Kerstin Zawatzky, Manfred Grieser, Oded Heber, Brandon Jordon-Thaden, Claude Krantz, Oldřich Novotný, Roland Repnow, Volker Schurig, Dirk Schwalm, Zeev Vager, Andreas Wolf, Oliver Trapp, and Holger Kreckel. Imaging the absolute configuration of a chiral epoxide in the gas phase. *Science*, 342(6162):1084–1086, 2013. doi: 10.1126/science.1246549. URL <https://www.science.org/doi/abs/10.1126/science.1246549>.
- [7] K. Mogyorosi, K. Sarosi, and V. Chikan. Direct production of ch(a2δ) radical from intense femtosecond near-ir laser pulses. *The Journal of Physical Chemistry A*, 124(40):8112–8119, Oct 2020. ISSN 1089-5639. doi: 10.1021/acs.jpca.0c05206. URL <https://doi.org/10.1021/acs.jpca.0c05206>.
- [8] Vaibhav Singh, Chuan Cheng, Thomas Weinacht, and Spiridoula Matsika. Quantum contributions to coulomb-explosion imaging revealed by trajectory-surface-hopping molecular dynamics. *Phys. Rev. A*, 109:052813, May 2024. doi: 10.1103/PhysRevA.109.052813. URL <https://link.aps.org/doi/10.1103/PhysRevA.109.052813>.
- [9] Weiwei Zhou, Lingfeng Ge, Graham A. Cooper, Stuart W. Crane, Michael H. Evans, Michael N. R. Ashfold, and Claire Vallance. Coulomb explosion imaging for gas-phase molecular structure determination: An ab initio trajectory simulation study. *The Journal of Chemical Physics*, 153(18):184201, 11 2020. ISSN 0021-9. doi: 10.1063/5.0024833. URL <https://doi.org/10.1063/5.0024833>.
- [10] Tomoyuki Yatsuhashi and Nobuaki Nakashima. Multiple ionization and coulomb explosion of molecules, molecular complexes, clusters and solid surfaces. *Journal of Photochemistry and Photobiology C: Photochemistry Reviews*, 34:52–84, 2018. ISSN 1389-5567. doi: <https://doi.org/10.1016/j.jphotochemrev.2017.12.001>. URL <https://www.sciencedirect.com/science/article/pii/S1389556717300680>.
- [11] Chengyin Wu, Yudong Yang, Zhifeng Wu, Bozhen Chen, Hua Dong, Xianrong Liu, Yongkai Deng, Hong Liu, Yunquan Liu, and Qihuang Gong. Coulomb explosion of nitrogen and oxygen molecules through non-coulombic states. *Phys. Chem. Chem. Phys.*, 13:18398–18408, 2011. doi: 10.1039/C1CP21345H. URL <http://dx.doi.org/10.1039/C1CP21345H>.
- [12] Louis Minion, Jason W. L. Lee, and Michael Burt. Predicting coulomb explosion fragment angular distributions using molecular ground-state vibrational motion. *PHYSICAL CHEMISTRY CHEMICAL PHYSICS*, 24(19):11636–11645, MAY 18 2022. doi: 10.1039/d2cp01114j.

- [13] Stuart W. Crane, Lingfeng Ge, Graham A. Cooper, Ben P. Carwithen, Matthew Bain, James A. Smith, Christopher S. Hansen, and Michael N. R. Ashfold. Nonadiabatic coupling effects in the 800 nm strong-field ionization-induced coulomb explosion of methyl iodide revealed by multimass velocity map imaging and ab initio simulation studies. *JOURNAL OF PHYSICAL CHEMISTRY A*, 125(44):9594–9608, NOV 11 2021. doi: 10.1021/acs.jpca.1c06346.
- [14] Akiyoshi Hishikawa, Akitaka Matsuda, Mizuho Fushitani, and Eiji J. Takahashi. Visualizing recurrently migrating hydrogen in acetylene dication by intense ultrashort laser pulses. *Phys. Rev. Lett.*, 99:258302, Dec 2007. doi: 10.1103/PhysRevLett.99.258302. URL <https://link.aps.org/doi/10.1103/PhysRevLett.99.258302>.
- [15] Pan Ma, Chuncheng Wang, Sizuo Luo, Xiaokai Li, Wenhui Hu, Jiaqi Yu, Xitao Yu, Xu Tian, Zexing Qu, and Dajun Ding. Bond-breakage-dependent dissociative ionization of an asymmetric molecule in an intense femtosecond laser field. *Phys. Rev. A*, 99:023423, Feb 2019. doi: 10.1103/PhysRevA.99.023423. URL <https://link.aps.org/doi/10.1103/PhysRevA.99.023423>.
- [16] M. E. Corrales, J. González-Vázquez, R. de Nalda, and L. Bañares. Coulomb explosion imaging for the visualization of a conical intersection. *The Journal of Physical Chemistry Letters*, 10(2):138–143, 2019. doi: 10.1021/acs.jpclett.8b03726. URL <https://doi.org/10.1021/acs.jpclett.8b03726>. PMID: 30561209.
- [17] Dror M. Bittner, Krishnendu Gope, Ester Livshits, Roi Baer, and Daniel Strasser. Sequential and concerted C–C and C–O bond dissociation in the Coulomb explosion of 2-propanol. *The Journal of Chemical Physics*, 157(7):074309, 08 2022. ISSN 0021-9606. doi: 10.1063/5.0098531. URL <https://doi.org/10.1063/5.0098531>.
- [18] Ming Zhang, Zhengning Guo, Xiaoyu Mi, Zheng Li, and Yunquan Liu. Ultrafast imaging of molecular dynamics using ultrafast low-frequency lasers, x-ray free electron lasers, and electron pulses. *The Journal of Physical Chemistry Letters*, 13(7):1668–1680, 2022. doi: 10.1021/acs.jpclett.1c03916. URL <https://doi.org/10.1021/acs.jpclett.1c03916>. PMID: 35147438.
- [19] Lorenz Kranabetter, Henrik H. Kristensen, Constant A. Schouder, and Henrik Stapelfeldt. Structure determination of alkali trimers on helium nanodroplets through laser-induced Coulomb explosion. *The Journal of Chemical Physics*, 160(13):131101, 04 2024. ISSN 0021-9606. doi: 10.1063/5.0200389. URL <https://doi.org/10.1063/5.0200389>.
- [20] Henrik H. Kristensen, Lorenz Kranabetter, Constant A. Schouder, Jacqueline Arlt, Frank Jensen, and Henrik Stapelfeldt. Laser-induced coulomb explosion imaging of alkali-metal dimers on helium nanodroplets. *Phys. Rev. A*, 107:023104, Feb 2023. doi: 10.1103/PhysRevA.107.023104. URL <https://link.aps.org/doi/10.1103/PhysRevA.107.023104>.
- [21] Daniel Rolles. Time-resolved experiments on gas-phase atoms and molecules with xuv and x-ray free-electron lasers. *Advances in Physics: X*, 8(1):2132182, 2023. doi: 10.1080/23746149.2022.2132182. URL <https://doi.org/10.1080/23746149.2022.2132182>.
- [22] Surjendu Bhattacharyya, Kurtis Borne, Farzaneh Ziaeef, Shashank Pathak, Enliang Wang, Anbu Selvam Venkatachalam, Xiang Li, Nathan Marshall, Kevin D. Carnes, Charles W. Fehrenbach, Travis Severt, Itzik Ben-Itzhak, Artem Rudenko, and Daniel Rolles. Strong-field-induced coulomb explosion imaging of tribromomethane. *JOURNAL OF PHYSICAL CHEMISTRY LETTERS*, 13(25):5845–5853, JUN 30 2022. doi: 10.1021/acs.jpclett.2c01007.
- [23] Chuan Cheng, Leszek J. Frasinski, Gonenc Mogol, Felix Allum, Andrew J. Howard, Daniel Rolles, Philip H. Bucksbaum, Mark Brouard, Ruaridh Forbes, and Thomas Weinacht. Multiparticle cumulant mapping for coulomb explosion imaging. *PHYSICAL REVIEW LETTERS*, 130(9), MAR 2 2023. doi: 10.1103/PhysRevLett.130.093001.

- [24] Andrew J. Howard, Mathew Britton, Zachary L. Streeter, Chuan Cheng, Ruaridh Forbes, Joshua L. Reynolds, Felix Allum, Gregory A. McCracken, Ian Gabalski, Robert R. Lucchese, C. William McCurdy, Thomas Weinacht, and Philip H. Bucksbaum. Filming enhanced ionization in an ultrafast triatomic slingshot. *COMMUNICATIONS CHEMISTRY*, 6(1), APR 27 2023. doi: 10.1038/s42004-023-00882-w.
- [25] James Unwin, Felix Allum, Mathew Britton, Ian Gabalski, Hubertus Bromberger, Mark Brouard, Philip H. Bucksbaum, Taran Driver, Nagitha Ekanayake, Diksha Garg, Eva Gougoula, David Heathcote, Andrew J. Howard, Paul Hockett, David M. P. Holland, Sonu Kumar, Chow-shing Lam, Jason W. L. Lee, Joseph McManus, Jochen Mikosch, Dennis Milesevic, Russell S. Minns, Christina C. Papadopoulou, Christopher Passow, Weronika O. Razmus, Anja Röder, Arnaud Rouzée, Michael Schuurman, Alcides Simao, Albert Stolow, Atia Tul-Noor, Claire Vallance, Tiffany Walmsley, Daniel Rolles, Benjamin Erk, Michael Burt, and Ruaridh Forbes. X-ray induced coulomb explosion imaging of transient excited-state structural rearrangements in cs₂. *Communications Physics*, 6(1):309, Oct 2023. ISSN 2399-3650. doi: 10.1038/s42005-023-01414-7. URL <https://doi.org/10.1038/s42005-023-01414-7>.
- [26] X. Li, A. Rudenko, M. S. Schöffler, N. Anders, Th. M. Baumann, S. Eckart, B. Erk, A. De Fanis, K. Fehre, R. Dörner, L. Foucar, S. Grundmann, P. Grychtol, A. Hartung, M. Hofmann, M. Ilchen, Ch. Janke, G. Kastirke, M. Kircher, K. Kubicek, M. Kunitski, T. Mazza, S. Meister, N. Melzer, J. Montano, V. Music, G. Nalin, Y. Ovcharenko, Ch. Passow, A. Pier, N. Rennhack, J. Rist, D. E. Rivas, I. Schlichting, L. Ph. H. Schmidt, Ph. Schmidt, J. Siebert, N. Strenger, D. Trabert, F. Trinter, I. Vela-Perez, R. Wagner, P. Walter, M. Weller, P. Ziolkowski, A. Czasch, D. Rolles, M. Meyer, T. Jahnke, and R. Boll. Coulomb explosion imaging of small polyatomic molecules with ultrashort x-ray pulses. *Phys. Rev. Res.*, 4:013029, Jan 2022. doi: 10.1103/PhysRevResearch.4.013029. URL <https://link.aps.org/doi/10.1103/PhysRevResearch.4.013029>.
- [27] Craig S. Slater, Sophie Blake, Mark Brouard, Alexandra Lauer, Claire Vallance, C. Sean Bohun, Lauge Christensen, Jens H. Nielsen, Mikael P. Johansson, and Henrik Stapelfeldt. Coulomb-explosion imaging using a pixel-imaging mass-spectrometry camera. *Phys. Rev. A*, 91:053424, May 2015. doi: 10.1103/PhysRevA.91.053424. URL <https://link.aps.org/doi/10.1103/PhysRevA.91.053424>.
- [28] Martin Pitzer, Maksim Kunitski, Allan S. Johnson, Till Jahnke, Hendrik Sann, Felix Sturm, Lothar Ph. H. Schmidt, Horst Schmidt-Böcking, Reinhard Dörner, Jürgen Stohner, Julia Kiedrowski, Michael Reggelin, Sebastian Marquardt, Alexander Schießer, Robert Berger, and Markus S. Schöffler. Direct determination of absolute molecular stereochemistry in gas phase by coulomb explosion imaging. *Science*, 341(6150):1096–1100, 2013. doi: 10.1126/science.1240362. URL <https://www.science.org/doi/abs/10.1126/science.1240362>.
- [29] Rebecca Boll, Julia M. Schäfer, Benoît Richard, Kilian Fehre, Gregor Kastirke, Zoltan Jurek, Markus S. Schöffler, Malik M. Abdullah, Nils Anders, Thomas M. Baumann, Sebastian Eckart, Benjamin Erk, Alberto De Fanis, Reinhard Dörner, Sven Grundmann, Patrik Grychtol, Alexander Hartung, Max Hofmann, Markus Ilchen, Ludger Inhester, Christian Janke, Rui Jin, Max Kircher, Katharina Kubicek, Maksim Kunitski, Xiang Li, Tommaso Mazza, Severin Meister, Niklas Melzer, Jacobo Montano, Valerija Music, Giammarco Nalin, Yevheniy Ovcharenko, Christopher Passow, Andreas Pier, Nils Rennhack, Jonas Rist, Daniel E. Rivas, Daniel Rolles, Ilme Schlichting, Lothar Ph. H. Schmidt, Philipp Schmidt, Juliane Siebert, Nico Strenger, Daniel Trabert, Florian Trinter, Isabel Vela-Perez, Rene Wagner, Peter Walter, Miriam Weller, Paweł Ziolkowski, Sang-Kil Son, Artem Rudenko, Michael Meyer, Robin Santra, and Till Jahnke. X-ray multiphoton-induced coulomb explosion images complex single molecules. *Nature Physics*, 18(4):423–428, Apr 2022. ISSN 1745-2481. doi: 10.1038/s41567-022-01507-0. URL <https://doi.org/10.1038/s41567-022-01507-0>.
- [30] Felix Allum, Michael Burt, Kasra Amini, Rebecca Boll, Hansjochen Köckert, Pavel K. Olshin, Sadia Bari, Cédric Bomme, Felix Brause, Barbara Cunha de Miranda, Stefan Düsterer, Benjamin Erk, Marie Géloc, Romain Geneaux, Alexander S. Gentleman, Gildas Goldsztejn, Renaud Guillemin, David M. P. Holland, Iyas Ismail, Per Johnsson, Loïc Journel, Jochen Küpper, Jan Lahl, Jason W. L. Lee, Sylvain Maclot, Stuart R. Mackenzie, Bastian Manschwetus, Andrey S. Mereshchenko, Robert Mason, Jérôme

- Palaudoux, Maria Novella Piancastelli, Francis Penent, Dimitrios Rompotis, Arnaud Rouzée, Thierry Ruchon, Artem Rudenko, Evgeny Savylyev, Marc Simon, Nora Schirmel, Henrik Stapelfeldt, Simone Techert, Oksana Travnikova, Sebastian Trippel, Jonathan G. Underwood, Claire Vallance, Joss Wiese, Farzaneh Ziae, Mark Brouard, Tatiana Marchenko, and Daniel Rolles. Coulomb explosion imaging of CH₃I and CH₂CII photodissociation dynamics. *The Journal of Chemical Physics*, 149(20):204313, 11 2018. ISSN 0021-9606. doi: 10.1063/1.5041381. URL <https://doi.org/10.1063/1.5041381>.
- [31] Tomoyuki Endo, Simon P. Neville, Vincent Wanie, Samuel Beaulieu, Chen Qu, Jude Deschamps, Philippe Lassonde, Bruno E. Schmidt, Hikaru Fujise, Mizuho Fushitani, Akiyoshi Hishikawa, Paul L. Houston, Joel M. Bowman, Michael S. Schuurman, François Légaré, and Heide Ibrahim. Capturing roaming molecular fragments in real time. *Science*, 370(6520):1072–1077, 2020. doi: 10.1126/science.abc2960. URL <https://www.science.org/doi/abs/10.1126/science.abc2960>.
 - [32] Sonia Erattupuzha, Cody L Covington, Arthur Russakoff, Erik Lötstedt, Seyedreza Larimian, Václav Hanus, Sergiy Bubin, Markus Koch, Stefanie Gräfe, Andrius Baltuška, Xinhua Xie, Kaoru Yamanouchi, Kálmán Varga, and Markus Kitzler. Enhanced ionisation of polyatomic molecules in intense laser pulses is due to energy upshift and field coupling of multiple orbitals. *Journal of Physics B: Atomic, Molecular and Optical Physics*, 50(12):125601, may 2017. doi: 10.1088/1361-6455/aa7098. URL <https://dx.doi.org/10.1088/1361-6455/aa7098>.
 - [33] F Légaré, Kevin F Lee, A D Bandrauk, D M Villeneuve, and P B Corkum. Laser coulomb explosion imaging for probing ultra-fast molecular dynamics. *Journal of Physics B: Atomic, Molecular and Optical Physics*, 39(13):S503, jun 2006. doi: 10.1088/0953-4075/39/13/S23. URL <https://dx.doi.org/10.1088/0953-4075/39/13/S23>.
 - [34] H. Stapelfeldt, E. Constant, and P. B. Corkum. Wave packet structure and dynamics measured by coulomb explosion. *Phys. Rev. Lett.*, 74:3780–3783, May 1995. doi: 10.1103/PhysRevLett.74.3780. URL <https://link.aps.org/doi/10.1103/PhysRevLett.74.3780>.
 - [35] XiaoQing Hu, YiGeng Peng, XiaoLong Zhu, ShunCheng Yan, Ling Liu, WenTian Feng, DaLong Guo, Yong Gao, ShaoFeng Zhang, DongMei Zhao, DaPu Dong, Bang Hai, JiaWei Xu, SongBin Zhang, X. Ma, JianGuo Wang, and Yong Wu. Breakdown of the coulomb-explosion imaging technique induced by the ultrafast rotation of fragments. *Phys. Rev. A*, 101:012707, Jan 2020. doi: 10.1103/PhysRevA.101.012707. URL <https://link.aps.org/doi/10.1103/PhysRevA.101.012707>.
 - [36] Xinyu Zhang, Xinning Zhao, Hui Liu, Zhongyu Yin, Xiaoge Zhao, Pan Ma, Xiaokai Li, Chuncheng Wang, Qinxin Wang, Sizuo Luo, and Dajun Ding. Ultrafast coulomb explosion of the nh₃sub₃⁺/sub₃dimer, trimer, and tetramer in strong laser fields. *PHYSICAL REVIEW A*, 109(2), FEB 15 2024. doi: 10.1103/PhysRevA.109.023112.
 - [37] Marcos Dantus. Ultrafast studies of elusive chemical reactions in the gas phase. *Science*, 385 (6709):eadk1833, 2024. doi: 10.1126/science.adk1833. URL <https://www.science.org/doi/abs/10.1126/science.adk1833>.
 - [38] Elio G. Champenois, Nanna H. List, Matthew Ware, Mathew Britton, Philip H. Bucksbaum, Xinxin Cheng, Martin Centurion, James P. Cryan, Ruaridh Forbes, Ian Gabalski, Kareem Hegazy, Matthias C. Hoffmann, Andrew J. Howard, Fuhao Ji, Ming-Fu Lin, J. Pedro F. Nunes, Xiaozhe Shen, Jie Yang, Xijie Wang, Todd J. Martinez, and Thomas J. A. Wolf. Femtosecond electronic and hydrogen structural dynamics in ammonia imaged with ultrafast electron diffraction. *Phys. Rev. Lett.*, 131:143001, Oct 2023. doi: 10.1103/PhysRevLett.131.143001. URL <https://link.aps.org/doi/10.1103/PhysRevLett.131.143001>.
 - [39] Stuart W. Crane, Jason W. L. Lee, Michael N. R. Ashfold, and Daniel Rolles. Molecular photodissociation dynamics revealed by coulomb explosion imaging. *Phys. Chem. Chem. Phys.*, 25:16672–16698, 2023. doi: 10.1039/D3CP01740K. URL <http://dx.doi.org/10.1039/D3CP01740K>.

- [40] Nagitha Ekanayake, Muath Nairat, Balram Kaderiya, Peyman Feizollah, Bethany Jochim, Travis Severt, Ben Berry, Kanaka Raju Pandiri, Kevin D. Carnes, Shashank Pathak, Daniel Rolles, Artem Rudenko, Itzik Ben-Itzhak, Christopher A. Mancuso, B. Scott Fales, James E. Jackson, Benjamin G. Levine, and Marcos Dantus. Mechanisms and time-resolved dynamics for trihydrogen cation (h_3^+) formation from organic molecules in strong laser fields. *Scientific Reports*, 7(1):4703, Jul 2017. ISSN 2045-2322. doi: 10.1038/s41598-017-04666-w. URL <https://doi.org/10.1038/s41598-017-04666-w>.
- [41] Nagitha Ekanayake, Travis Severt, Muath Nairat, Nicholas P. Weingartz, Benjamin M. Farris, Balram Kaderiya, Peyman Feizollah, Bethany Jochim, Farzaneh Ziae, Kurtis Borne, Kanaka Raju P., Kevin D. Carnes, Daniel Rolles, Artem Rudenko, Benjamin G. Levine, James E. Jackson, Itzik Ben-Itzhak, and Marcos Dantus. H₂ roaming chemistry and the formation of h₃⁺ from organic molecules in strong laser fields. *Nature Communications*, 9(1):5186, Dec 2018. ISSN 2041-1723. doi: 10.1038/s41467-018-07577-0. URL <https://doi.org/10.1038/s41467-018-07577-0>.
- [42] T. Ditmire, T. Donnelly, R. W. Falcone, and M. D. Perry. Strong x-ray emission from high-temperature plasmas produced by intense irradiation of clusters. *Phys. Rev. Lett.*, 75:3122–3125, Oct 1995. doi: 10.1103/PhysRevLett.75.3122. URL <https://link.aps.org/doi/10.1103/PhysRevLett.75.3122>.
- [43] A. McPherson, B. D. Thompson, A. B. Borisov, K. Boyer, and C. K. Rhodes. Multiphoton-induced x-ray emission at 4–5 kev from xe atoms with multiple core vacancies. *Nature*, 370(6491):631–634, Aug 1994. ISSN 1476-4687. doi: 10.1038/370631a0. URL <https://doi.org/10.1038/370631a0>.
- [44] Y. L. Shao, T. Ditmire, J. W. G. Tisch, E. Springate, J. P. Marangos, and M. H. R. Hutchinson. Multi-kev electron generation in the interaction of intense laser pulses with xe clusters. *Phys. Rev. Lett.*, 77:3343–3346, Oct 1996. doi: 10.1103/PhysRevLett.77.3343. URL <https://link.aps.org/doi/10.1103/PhysRevLett.77.3343>.
- [45] J. Zweibaum, R. A. Smith, T. E. Cowan, G. Hays, K. B. Wharton, V. P. Yanovsky, and T. Ditmire. Nuclear fusion driven by coulomb explosions of large deuterium clusters. *Phys. Rev. Lett.*, 84:2634–2637, Mar 2000. doi: 10.1103/PhysRevLett.84.2634. URL <https://link.aps.org/doi/10.1103/PhysRevLett.84.2634>.
- [46] Isidore Last and Joshua Jortner. Nuclear fusion driven by coulomb explosion of methane clusters. *The Journal of Physical Chemistry A*, 106(45):10877–10885, Nov 2002. ISSN 1089-5639. doi: 10.1021/jp0206121. URL <https://doi.org/10.1021/jp0206121>.
- [47] Joshua Jortner and Isidore Last. Nuclear fusion driven by coulomb explosion of molecular clusters. *ChemPhysChem*, 3(10):845–848, 2002. doi: [https://doi.org/10.1002/1439-7641\(20021018\)3:10<845::AID-CPHC845>3.0.CO;2-P](https://doi.org/10.1002/1439-7641(20021018)3:10<845::AID-CPHC845>3.0.CO;2-P). URL <https://chemistry-europe.onlinelibrary.wiley.com/doi/abs/10.1002/1439-7641%2820021018%293%3A10%3C845%3A%3AAID-CPHC845%3E3.0.CO%3B2-P>.
- [48] Isidore Last and Joshua Jortner. Nuclear fusion driven by coulomb explosion of homonuclear and heteronuclear deuterium- and tritium-containing clusters. *Phys. Rev. A*, 64:063201, Nov 2001. doi: 10.1103/PhysRevA.64.063201. URL <https://link.aps.org/doi/10.1103/PhysRevA.64.063201>.
- [49] Isidore Last and Joshua Jortner. Energetics at extremes in coulomb explosion of large finite systems. *Chemical Physics*, 399:218–223, 2012. ISSN 0301-0104. doi: <https://doi.org/10.1016/j.chemphys.2011.11.026>. URL <https://www.sciencedirect.com/science/article/pii/S0301010411005210>. New trends in atomic and molecular clusters.
- [50] Isidore Last and Joshua Jortner. Nuclear fusion induced by coulomb explosion of heteronuclear clusters. *Phys. Rev. Lett.*, 87:033401, Jun 2001. doi: 10.1103/PhysRevLett.87.033401. URL <https://link.aps.org/doi/10.1103/PhysRevLett.87.033401>.
- [51] Isidore Last, Shlomo Ron, Andreas Heidenreich, and Joshua Jortner. Coulomb explosion of nanodroplets drives the conversion of laser energy to nuclear energy. *High Power Laser Science and Engineering*, 1(2):69–73, 2013. doi: 10.1017/hpl.2013.10.

- [52] Shlomo Ron, Isidore Last, and Joshua Jortner. Nuclear fusion of deuterons with light nuclei driven by coulomb explosion of nanodroplets. *Physics of Plasmas*, 19(11):112707, 11 2012. ISSN 1070-664X. doi: 10.1063/1.4766755. URL <https://doi.org/10.1063/1.4766755>.
- [53] Akiyoshi Hishikawa, Atsushi Iwamae, Kennosuke Hoshina, Mitsuhiro Kono, and Kaoru Yamanouchi. Coulomb explosion dynamics of n₂o in intense laser-field: Identification of new two-body and three-body fragmentation pathways. *Research on Chemical Intermediates*, 24(7):765–784, Jul 1998. ISSN 1568-5675. doi: 10.1163/156856798X00401. URL <https://doi.org/10.1163/156856798X00401>.
- [54] Martin Pitzer, Gregor Kastirke, Maksim Kunitski, Till Jahnke, Tobias Bauer, Christoph Goihl, Florian Trinter, Carl Schober, Kevin Henrichs, Jasper Becht, Stefan Zeller, Helena Gassert, Markus Waitz, Andreas Kuhlins, Hendrik Sann, Felix Sturm, Florian Wiegandt, Robert Wallauer, Lothar Ph. H. Schmidt, Allan S. Johnson, Manuel Mazenauer, Benjamin Spenger, Sabrina Marquardt, Sebastian Marquardt, Horst Schmidt-Böcking, Jürgen Stohner, Reinhard Dörner, Markus Schöffler, and Robert Berger. Absolute configuration from different multifragmentation pathways in light-induced coulomb explosion imaging. *ChemPhysChem*, 17(16):2465–2472, 2016. doi: <https://doi.org/10.1002/cphc.201501118>. URL <https://chemistry-europe.onlinelibrary.wiley.com/doi/abs/10.1002/cphc.201501118>.
- [55] Itamar Luzon, Ester Livshits, Krishnendu Gope, Roi Baer, and Daniel Strasser. Making sense of coulomb explosion imaging. *The Journal of Physical Chemistry Letters*, 10(6):1361–1367, Mar 2019. doi: 10.1021/acs.jpclett.9b00576. URL <https://doi.org/10.1021/acs.jpclett.9b00576>.
- [56] Surjendu Bhattacharyya, Kurtis Borne, Farzaneh Ziaeef, Shashank Pathak, Enliang Wang, Anbu Selvam Venkatachalam, Xiang Li, Nathan Marshall, Kevin D. Carnes, Charles W. Fehrenbach, Travis Severt, Itzik Ben-Itzhak, Artem Rudenko, and Daniel Rolles. Strong-field-induced coulomb explosion imaging of tribromomethane. *The Journal of Physical Chemistry Letters*, 13(25):5845–5853, Jun 2022. doi: 10.1021/acs.jpclett.2c01007. URL <https://doi.org/10.1021/acs.jpclett.2c01007>.
- [57] Hua Wu, Yuanxin Xue, Junqing Wen, Hui Wang, Qingfei Fan, Guoxiang Chen, Jin Zhu, Fanghui Qu, and Jiale Guo. Theoretical and experimental studies on hydrogen migration in dissociative ionization of the methanol monocation to molecular ions h₃⁺ and h₂o⁺. *RSC Adv.*, 9:16683–16689, 2019. doi: 10.1039/C9RA02003A. URL <http://dx.doi.org/10.1039/C9RA02003A>.
- [58] Huiliang Xu, Tomoya Okino, and Kaoru Yamanouchi. Ultrafast hydrogen migration in allene in intense laser fields: Evidence of two-body coulomb explosion. *Chemical Physics Letters*, 469(4): 255–260, 2009. ISSN 0009-2614. doi: <https://doi.org/10.1016/j.cplett.2008.12.097>. URL <https://www.sciencedirect.com/science/article/pii/S0009261409000049>.
- [59] Huiliang Xu, Tomoya Okino, Katsunori Nakai, Kaoru Yamanouchi, Stefan Roither, Xinhua Xie, Daniil Kartashov, Markus Schöffler, Andrius Baltuska, and Markus Kitzler. Hydrogen migration and c–c bond breaking in 1,3-butadiene in intense laser fields studied by coincidence momentum imaging. *Chemical Physics Letters*, 484(4):119–123, 2010. ISSN 0009-2614. doi: <https://doi.org/10.1016/j.cplett.2009.11.008>. URL <https://www.sciencedirect.com/science/article/pii/S0009261409014146>.
- [60] Peter M. Kraus, Martin C. Schwarzer, Nora Schirmel, Gunter Urbasch, Gernot Frenking, and Karl-Michael Weitzel. Unusual mechanism for H₃⁺ formation from ethane as obtained by femtosecond laser pulse ionization and quantum chemical calculations. *The Journal of Chemical Physics*, 134(11):114302, 03 2011. ISSN 0021-9606. doi: 10.1063/1.3561311. URL <https://doi.org/10.1063/1.3561311>.
- [61] Travis Severt, Eleanor Weckwerth, Balram Kaderiya, Peyman Feizollah, Bethany Jochim, Kurtis Borne, Farzaneh Ziaeef, Kanaka Raju P, Kevin D. Carnes, Marcos Dantus, Daniel Rolles, Artem Rudenko, Eric Wells, and Itzik Ben-Itzhak. Initial-site characterization of hydrogen migration following strong-field double-ionization of ethanol. *Nature Communications*, 15(1):74, Jan 2024. ISSN 2041-1723. doi: 10.1038/s41467-023-44311-x. URL <https://doi.org/10.1038/s41467-023-44311-x>.
- [62] Sung Kwon, Shawn Sandhu, Moaid Shaik, Jacob Stamm, Jesse Sandhu, Rituparna Das, Caitlin V. Hetherington, Benjamin G. Levine, and Marcos Dantus. What is the mechanism of h₃⁺ formation from cyclopropane? *The Journal of Physical Chemistry A*, 127(41):8633–8638, Oct 2023. ISSN 1089-5639. doi: 10.1021/acs.jpca.3c05442. URL <https://doi.org/10.1021/acs.jpca.3c05442>.

- [63] Matthew J. Michie, Nagitha Ekanayake, Nicholas P. Weingartz, Jacob Stamm, and Marcos Dantus. Quantum coherent control of h₃⁺ formation in strong fields. *The Journal of Chemical Physics*, 150(4):044303, 01 2019. ISSN 0021-9606. doi: 10.1063/1.5070067. URL <https://doi.org/10.1063/1.5070067>.
- [64] C Cornaggia, D Normand, and J Morellec. Role of the molecular electronic configuration in the coulomb fragmentation of n₂, c₂h₂ and c₂h₄ in an intense laser field. *Journal of Physics B: Atomic, Molecular and Optical Physics*, 25(17):L415, sep 1992. doi: 10.1088/0953-4075/25/17/003. URL <https://dx.doi.org/10.1088/0953-4075/25/17/003>.
- [65] Stefan Roither, Xinhua Xie, Daniil Kartashov, Li Zhang, Markus Schöffler, Huiliang Xu, Atsushi Iwasaki, Tomoya Okino, Kaoru Yamanouchi, Andrius Baltuska, and Markus Kitzler. High energy proton ejection from hydrocarbon molecules driven by highly efficient field ionization. *Phys. Rev. Lett.*, 106:163001, Apr 2011. doi: 10.1103/PhysRevLett.106.163001. URL <https://link.aps.org/doi/10.1103/PhysRevLett.106.163001>.
- [66] Alexei N. Markevitch, Dmitri A. Romanov, Stanley M. Smith, and Robert J. Levis. Coulomb explosion of large polyatomic molecules assisted by nonadiabatic charge localization. *Phys. Rev. Lett.*, 92:063001, Feb 2004. doi: 10.1103/PhysRevLett.92.063001. URL <https://link.aps.org/doi/10.1103/PhysRevLett.92.063001>.
- [67] C. Cornaggia, M. Schmidt, and D. Normand. Laser-induced nuclear motions in the coulomb explosion of c₂h₂⁺ ions. *Phys. Rev. A*, 51:1431–1437, Feb 1995. doi: 10.1103/PhysRevA.51.1431. URL <https://link.aps.org/doi/10.1103/PhysRevA.51.1431>.
- [68] Seiji Shimizu, Junkei Kou, Sakae Kawato, Keisuke Shimizu, Shuji Sakabe, and Nobuaki Nakashima. Coulomb explosion of benzene irradiated by an intense femtosecond laser pulse. *Chemical Physics Letters*, 317(6):609–614, 2000. ISSN 0009-2614. doi: [https://doi.org/10.1016/S0009-2614\(99\)01376-7](https://doi.org/10.1016/S0009-2614(99)01376-7). URL <https://www.sciencedirect.com/science/article/pii/S0009261499013767>.
- [69] Sasi Palaniyappan, Rob Mitchell, N. Ekanayake, A. M. Watts, S. L. White, Rob Sauer, L. E. Howard, M. Vidotto, C. Mancuso, S. J. Wells, T. Stanev, B. L. Wen, M. F. Decamp, and B. C. Walker. Ionization of ethane, butane, and octane in strong laser fields. *Phys. Rev. A*, 82:043433, Oct 2010. doi: 10.1103/PhysRevA.82.043433. URL <https://link.aps.org/doi/10.1103/PhysRevA.82.043433>.
- [70] Janpieter Van Dijk. *Unravelling the Maze of Scientific Writing Through the Ages - On the Origins of the Terms Hydrocarbon, Petroleum, Natural Gas, and Methane*. 10 2022. ISBN ISBN 9798353989172.
- [71] Masseron, T., Plez, B., Van Eck, S., Colin, R., Daoutidis, I., Godefroid, M., Coheur, P.-F., Bernath, P., Jorissen, A., and Christlieb, N. Ch in stellar atmospheres: an extensive linelist. *AA*, 571:A47, 2014. doi: 10.1051/0004-6361/201423956. URL <https://doi.org/10.1051/0004-6361/201423956>.
- [72] Jonathan Tennyson. *Astronomical Spectroscopy*. WORLD SCIENTIFIC, 2nd edition, 2011. doi: 10.1142/7574. URL <https://www.worldscientific.com/doi/abs/10.1142/7574>.
- [73] Huynh Van Sa Lam, Anbu Selvam Venkatachalam, Surjendu Bhattacharyya, Keyu Chen, Kurtis Borne, Enliang Wang, Rebecca Boll, Till Jahnke, Vinod Kumarappan, Artem Rudenko, and Daniel Rolles. Differentiating three-dimensional molecular structures using laser-induced coulomb explosion imaging. *Phys. Rev. Lett.*, 132:123201, Mar 2024. doi: 10.1103/PhysRevLett.132.123201. URL <https://link.aps.org/doi/10.1103/PhysRevLett.132.123201>.
- [74] Huynh Van Sa Lam, Van-Hung Hoang, Anbu Selvam Venkatachalam, Surjendu Bhattacharyya, Keyu Chen, Sina Jacob, Sanduni Kudagama, Tu Thanh Nguyen, Daniel Rolles, Uwe Thumm, Artem Rudenko, and Vinod Kumarappan. Imaging coupled vibrational, rotational, and electronic wave packet dynamics in a triatomic molecule. 2024. URL <https://arxiv.org/abs/2408.07958>.
- [75] Kasra Amini, Rebecca Boll, Alexandra Lauer, Michael Burt, Jason W. L. Lee, Lauge Christensen, Felix Braue, Terence Mullins, Evgeny Savelyev, Utuq Ablikim, Nora Berrah, Cédric Bomme, Stefan Düsterer, Benjamin Erk, Hauke Höppner, Per Johnsson, Thomas Kierspel, Faruk Krecinic, Jochen Küpper, Maria

- Müller, Erland Müller, Harald Redlin, Arnaud Rouzée, Nora Schirmel, Jan Thøgersen, Simone Techert, Sven Toleikis, Rolf Treusch, Sebastian Trippel, Anatoli Ulmer, Joss Wiese, Claire Vallance, Artem Rudenko, Henrik Stapelfeldt, Mark Brouard, and Daniel Rolles. Alignment, orientation, and Coulomb explosion of difluoroiodobenzene studied with the pixel imaging mass spectrometry (PImMS) camera. *The Journal of Chemical Physics*, 147(1):013933, 05 2017. ISSN 0021-9606. doi: 10.1063/1.4982220. URL <https://doi.org/10.1063/1.4982220>.
- [76] Utuq Ablikim, Cédric Bomme, Evgeny Savelyev, Hui Xiong, Rajesh Kushawaha, Rebecca Boll, Kasra Amini, Timur Osipov, David Kilcoyne, Artem Rudenko, Nora Berrah, and Daniel Rolles. Isomer-dependent fragmentation dynamics of inner-shell photoionized difluoroiodobenzene. *Phys. Chem. Chem. Phys.*, 19:13419–13431, 2017. doi: 10.1039/C7CP01379E. URL <http://dx.doi.org/10.1039/C7CP01379E>.
- [77] F. Légaré, Kevin F. Lee, I. V. Litvinyuk, P. W. Dooley, S. S. Wesolowski, P. R. Bunker, P. Dombi, F. Krausz, A. D. Bandrauk, D. M. Villeneuve, and P. B. Corkum. Laser coulomb-explosion imaging of small molecules. *Phys. Rev. A*, 71:013415, Jan 2005. doi: 10.1103/PhysRevA.71.013415. URL <https://link.aps.org/doi/10.1103/PhysRevA.71.013415>.
- [78] Akitaka Matsuda, Mizuho Fushitani, Eiji J. Takahashi, and Akiyoshi Hishikawa. Visualizing hydrogen atoms migrating in acetylene dication by time-resolved three-body and four-body coulomb explosion imaging. *Phys. Chem. Chem. Phys.*, 13:8697–8704, 2011. doi: 10.1039/C0CP02333G. URL <http://dx.doi.org/10.1039/C0CP02333G>.
- [79] Michael Burt, Rebecca Boll, Jason W. L. Lee, Kasra Amini, Hansjochen Köckert, Claire Vallance, Alexander S. Gentleman, Stuart R. Mackenzie, Sadia Bari, Cédric Bomme, Stefan Düsterer, Benjamin Erk, Bastian Manschwetus, Erland Müller, Dimitrios Rompotis, Evgeny Savelyev, Nora Schirmel, Simone Techert, Rolf Treusch, Jochen Küpper, Sebastian Trippel, Joss Wiese, Henrik Stapelfeldt, Barbara Cunha de Miranda, Renaud Guillemin, Iyas Ismail, Loïc Journel, Tatiana Marchenko, Jérôme Palaudoux, Francis Penent, Maria Novella Piancastelli, Marc Simon, Oksana Travnikova, Felix Brausse, Gildas Goldsztejn, Arnaud Rouzée, Marie Géléc, Romain Geneaux, Thierry Ruchon, Jonathan Underwood, David M. P. Holland, Andrey S. Mereshchenko, Pavel K. Olshin, Per Johnsson, Sylvain Maclot, Jan Lahl, Artem Rudenko, Farzaneh Ziaeef, Mark Brouard, and Daniel Rolles. Coulomb-explosion imaging of concurrent ch_2BrI photodissociation dynamics. *Phys. Rev. A*, 96:043415, Oct 2017. doi: 10.1103/PhysRevA.96.043415. URL <https://link.aps.org/doi/10.1103/PhysRevA.96.043415>.
- [80] Constant Schouder, Adam S Chatterley, Melby Johny, Flora Hübschmann, Ahmed F Al-Refaie, Florent Calvo, Jochen Küpper, and Henrik Stapelfeldt. Laser-induced coulomb explosion imaging of (c6h5br)2 and c6h5br-i2 dimers in helium nanodroplets using a tpx3cam. *Journal of Physics B: Atomic, Molecular and Optical Physics*, 54(18):184001, oct 2021. doi: 10.1088/1361-6455/ac04c4. URL <https://dx.doi.org/10.1088/1361-6455/ac04c4>.
- [81] A. Méry, V. Kumar, X. Fléchard, B. Gervais, S. Guillous, M. Lalande, J. Rangama, W. Wolff, and A. Cassimi. Coulomb-explosion imaging of carbon monoxide dimers. *Phys. Rev. A*, 103:042813, Apr 2021. doi: 10.1103/PhysRevA.103.042813. URL <https://link.aps.org/doi/10.1103/PhysRevA.103.042813>.
- [82] Tomas André, Emiliano De Santis, Nicusor Timneanu, and Carl Caleman. Partial orientation retrieval of proteins from coulomb explosions, 2024. URL <https://arxiv.org/abs/2410.15965>.
- [83] Tomas André, Ibrahim Dawod, Sebastian Cardoch, Emiliano De Santis, Nicusor Timneanu, and Carl Caleman. Protein structure classification based on x-ray laser induced coulomb explosion, 2024. URL <https://arxiv.org/abs/2410.15934>.
- [84] Yijue Ding, Loren Greenman, and Daniel Rolles. Surface hopping molecular dynamics simulation of ultrafast methyl iodide photodissociation mapped by coulomb explosion imaging. *PHYSICAL CHEMISTRY CHEMICAL PHYSICS*, 26(34):22423–22432, AUG 28 2024. doi: 10.1039/d4cp01679c.

- [85] María E. Corrales, Gregory Gitzinger, Jesús González-Vázquez, Vincent Loriot, Rebeca de Nalda, and Luis Bañares. Velocity map imaging and theoretical study of the coulomb explosion of ch₃i under intense femtosecond ir pulses. *The Journal of Physical Chemistry A*, 116(11):2669–2677, Mar 2012. ISSN 1089-5639. doi: 10.1021/jp207367a. URL <https://doi.org/10.1021/jp207367a>.
- [86] Satoshi Ohmura, Kiyonobu Nagaya, Fuyuki Shimojo, and Makoto Yao. Dissociation mechanism from highly charged bromophenol: ab initio molecular dynamics simulations. *Zeitschrift für Physikalische Chemie*, 235(1-2):169–187, 2021. doi: doi:10.1515/zpch-2020-1634. URL <https://doi.org/10.1515/zpch-2020-1634>.
- [87] Arthur Russakoff and Kálmán Varga. Time-dependent density-functional study of the ionization and fragmentation of c₂h₂ and h₂ by strong circularly polarized laser pulses. *Phys. Rev. A*, 92:053413, Nov 2015. doi: 10.1103/PhysRevA.92.053413. URL <https://link.aps.org/doi/10.1103/PhysRevA.92.053413>.
- [88] Cody Covington, Kara Hartig, Arthur Russakoff, Ryan Kulpins, and Kálmán Varga. Time-dependent density-functional-theory investigation of the collisions of protons and α particles with uracil and adenine. *Phys. Rev. A*, 95:052701, May 2017. doi: 10.1103/PhysRevA.95.052701. URL <https://link.aps.org/doi/10.1103/PhysRevA.95.052701>.
- [89] Arthur Russakoff, Sergiy Bubin, Xinhua Xie, Sonia Erattupuzha, Markus Kitzler, and Kálmán Varga. Time-dependent density-functional study of the alignment-dependent ionization of acetylene and ethylene by strong laser pulses. *Phys. Rev. A*, 91:023422, Feb 2015. doi: 10.1103/PhysRevA.91.023422. URL <https://link.aps.org/doi/10.1103/PhysRevA.91.023422>.
- [90] Xinhua Xie, Stefan Roither, Markus Schöffler, Huailiang Xu, Sergiy Bubin, Erik Lötstedt, Sonia Erattupuzha, Atsushi Iwasaki, Daniil Kartashov, Kálmán Varga, Gerhard G. Paulus, Andrius Baltuška, Kaoru Yamanouchi, and Markus Kitzler. Role of proton dynamics in efficient photoionization of hydrocarbon molecules. *Phys. Rev. A*, 89:023429, Feb 2014. doi: 10.1103/PhysRevA.89.023429. URL <https://link.aps.org/doi/10.1103/PhysRevA.89.023429>.
- [91] Sergiy Bubin, Mackenzie Atkinson, Kálmán Varga, Xinhua Xie, Stefan Roither, Daniil Kartashov, Andrius Baltuška, and Markus Kitzler. Strong laser-pulse-driven ionization and coulomb explosion of hydrocarbon molecules. *Phys. Rev. A*, 86:043407, Oct 2012. doi: 10.1103/PhysRevA.86.043407. URL <https://link.aps.org/doi/10.1103/PhysRevA.86.043407>.
- [92] Erich Runge and E. K. U. Gross. Density-functional theory for time-dependent systems. *Phys. Rev. Lett.*, 52:997–1000, Mar 1984. doi: 10.1103/PhysRevLett.52.997. URL <https://link.aps.org/doi/10.1103/PhysRevLett.52.997>.
- [93] Carsten A. Ullrich. *Time-Dependent Density-Functional Theory: Concepts and Applications*. Oxford University Press, Oxford, 1911.
- [94] Shuai Li, Diego Sierra-Costa, Matthew J. Michie, Itzik Ben-Itzhak, and Marcos Dantus. Control of electron recollision and molecular nonsequential double ionization. *Communications Physics*, 3(1): 35, Feb 2020. ISSN 2399-3650. doi: 10.1038/s42005-020-0297-3. URL <https://doi.org/10.1038/s42005-020-0297-3>.
- [95] Karoly Mogyorosi, Balint Toth, Krisztina Sarosi, Barnabas Gilicze, Janos Csontos, Tamas Somoskoi, Szabolcs Toth, Prasannan Geetha Prabhush, Laszlo Toth, Samuel Taylor, Nicholas Skoufis, Liam Baron, Kalman Varga, Cody Covington, and Viktor Chikan. Ch(a) radical formation in coulomb explosion from butane seeded plasma generated with chirp-controlled ultrashort laser pulses. *submitted for publication*, 2024.
- [96] Kálmán Varga and Joseph A. Driscoll. *Monte Carlo calculations*. Cambridge University Press, 2011.
- [97] N. Troullier and José Luís Martins. Efficient pseudopotentials for plane-wave calculations. *Phys. Rev. B*, 43:1993–2006, Jan 1991. doi: 10.1103/PhysRevB.43.1993. URL <https://link.aps.org/doi/10.1103/PhysRevB.43.1993>.

- [98] J. P. Perdew and Alex Zunger. Self-interaction correction to density-functional approximations for many-electron systems. *Phys. Rev. B*, 23:5048–5079, May 1981. doi: 10.1103/PhysRevB.23.5048. URL <https://link.aps.org/doi/10.1103/PhysRevB.23.5048>.
- [99] David E. Manolopoulos. Derivation and reflection properties of a transmission-free absorbing potential. *The Journal of Chemical Physics*, 117(21):9552–9559, 12 2002. ISSN 0021-9606. doi: 10.1063/1.1517042. URL <https://doi.org/10.1063/1.1517042>.